ISSN 1330-3651 (Print), ISSN 1848-6339 (Online)
https://doi.org/10.17559/TV-20241025002092
Original scientific paper

Novel Ten-Port MIMO Antenna with Enhanced Polarization Diversity for 5G Applications

R. S. MATHU BALA*, K. THENMALAR

Abstract: This design presents a novel ten-port Multi-Input Multi-Output (MIMO) antenna tailored for 5G smartphone applications. The antenna features a distinctive notched radiator etched on the ground plane, enabling operation within the 3.3 - 3.8 GHz frequency range, which is critical for 5G connectivity. To achieve desirable polarization diversity, the locations of the ten antenna elements were strategically chosen, significantly minimizing the coupling error rate and enhancing overall performance. The antenna's performance was rigorously validated through the fabrication of a prototype, ensuring that simulation results closely matched real-world outcomes. Comprehensive testing revealed excellent performance across the intended operating bandwidth with a reflection coefficient greater than 10 dB, ensuring effective impedance matching. Additionally, isolation between the antenna ports exceeded 20 dB, which is crucial for maintaining signal integrity in MIMO systems. The antenna also demonstrated impressive radiation efficiency, exceeding 74%, and a minimum correlation coefficient (*ECC*) of less than 0.03, indicating low correlation between antenna elements and thus enhancing MIMO capability. Furthermore, the study evaluated the impact of the human hand on Specific Absorption Rate (*SAR*) to assess safety and performance in practical usage scenarios. This comprehensive analysis of the ten-port MIMO antenna underscores its potential for integration into future 5G smartphones, balancing performance, efficiency, and user safety.

Keywords: 5G applications; coupling reduction; MIMO antenna; polarization diversity; Specific Absorption Rate (*SAR*)

1 INTRODUCTION

MIMO systems in fifth-generation (5G) mobile communication could greatly improve system throughput and quality of service (QoS) when compared to other generation systems used in 4G mobile networks [1, 2]. This has been significant because it enhances the data speeds and efficiency while preserving transmission capacity and bandwidth. In [3], the proposed antenna occupies overall individual antenna element size 7 × 12 mm^2 with impedance bandwidth of −6 dB across the operating bandwidth 3.4 - 3.6 GHz along with radiation efficiency of 46 - 68%. The radiation efficiency achieved up to 78% with mutual coupling less than 10 dB [4]. As a result, it is a practical solution that might be implemented in future communication systems [5]. The decoupling rate has been considered as highly important to improve the diversity ratio.

For 5G MIMO at 6 GHz frequency, this is currently enough. However, the isolation level needs to be increased to be higher than 15 to 20 dB in order to attain better MIMO performance. This is a difficult problem for 5G antenna arrays. Several extrinsic decoupling approaches, such as partial ground, etched slot, neutralization line (NL), parasitic scattered, and electromagnetic bandgap architecture [6], have been recently developed. Despite the fact that all these decoupling mechanisms improve isolation, a few of these designs will generally result in substantial performance degradation in fully integrated 5G MIMO arrays [7]. To put it another way, an increase in isolation typically comes at the expense of antenna efficiency. It is possible to achieve better performance in terms of isolation and efficiency with no use dedicated isolation enhancing mechanisms [8, 9]. The loss of efficiency while devising a unique way to design a 5G antenna, is proving tough [10, 11].

The overall dimension of the individual antenna elements is much higher which causes limited space availability to accommodate more antennas onto system board and also affects the radiation efficiency [12-15]. The general design of mobile phones severely determines the quantity of available space on them. Due to this, all the components in mobile board are affected by coupling. This can be avoided by providing proper isolation between the components in mobile board for 5G applications. All the antennas in the MIMO system cover frequency spectrum from 3.32 - 3.62 GHz in this paper. The coupling value is well below −20 dB without exploiting extrinsic decoupling mechanisms. Moreover, the antenna has channel capacity around 51.8 bps/Hz across the operating bandwidth which is 5 times higher than the 2 × 2 MIMO antenna systems. The effectiveness for the designed antenna has been evaluated by typical MIMO parameters. Further, the effect of the proposed 5G mobile antenna system is analyzed by including the antenna structure with the human hand phantom.

The manufacturing of mobile phone MIMO antennas involves several challenges that affect their practical implementation. One of the main issues lies in material selection, as substrates like FR4, commonly used for their cost-effectiveness, may introduce higher losses at high frequencies, impacting antenna performance. Alternative low-loss materials, such as ceramic or specialized polymers, can address this but are often expensive and complex to integrate into large-scale production. Additionally, precise alignment and integration of multiple antennas within the limited space of a mobile device require advanced fabrication techniques, such as laser or photolithography, which increase production costs and complexity. Achieving consistent impedance matching and low mutual coupling between antennas is another critical challenge, as it requires tight control over component tolerances and spacing, especially in compact form factors. Consequently, balancing performance and manufacturability in MIMO antenna design is essential to meeting practical requirements for commercial viability.

2 DESIGN METHODOLOGIES

2.1 Existing Method

Fig. 1 depicts the structure of the existing mobile pattern method and as described in the previous study operates solely at 3.4 - 3.6 GHz, exhibiting a Voltage Standing Wave Ratio (VSWR) of 3:1. It causes lagging in throughput of overall performance of the antenna. The overall dimension of printed circuit board is 136 × 68 × 1.6 mm^3 which is not quietly used for practical applications. The mutual coupling has been attained only below −13 dB. The existing design used only six antenna elements which were used in MIMO system, the achieved channel capacity across the operating bandwidth around 31.25 bps/Hz.

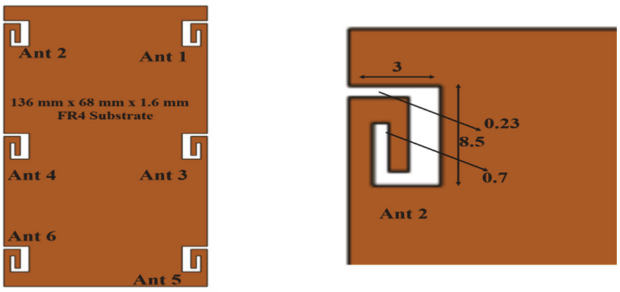

Figure 1 Overall structure of the existing method

2.2 Proposed Antenna Geometry and Analysis

Fig. 2a depicts the ten-port-antenna array for 5G with its general construction and design. The FR4 substrate's ground plane is etched with 10 identical open-ended slotted antennas. As seen in figure, they are all positioned symmetrically on the substrate's two long side edges. Fig. 2a. An L-shaped feeding line etched on the substrate's other side excites each antenna. The individual elements of the design are depicted in Fig. 2b. The radiating slots are obtained after connecting two rectangular slots together with dimensions 9.3 × 2.5 mm^2 and 3 × 0.7 mm^2 respectively. On the other hand, feed line is formed by connecting two rectangular blocks of dimension 3 × 0.7 mm^2, as pictorized in Fig. 2b.

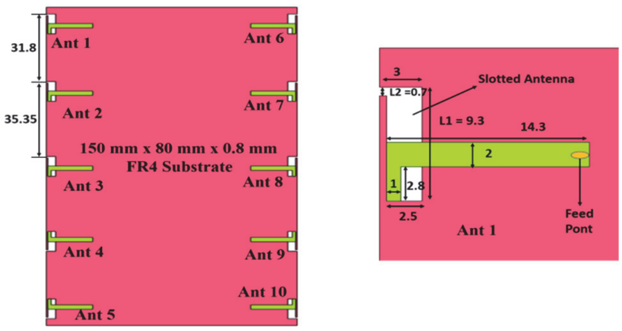

Figure 2 (a) Overall antenna Struture and its dimension (b) Individual antenna and its dimesion (Antenna 1)

3 PARAMETRIC ANALYSIS

3.1 Reflection and Transmission Coefficients

The scattering coefficients of *Ant*1 - *Ant*5 have been depicted in Fig. 3a to Fig. 3b. As illustrated, all the antennas have the frequency spectrum ranging from 3.3 - 3.8 GHz with −6 dB impedance bandwidth. Whereas, the antenna array functioned at 3.4 - 3.6 GHz covering the complete spectrum of LTE band 42. Fig. 4 shows the simulated and transmission co-efficients, respectively. To have better MIMO performance, isolation between antenna elements should be lower than −10dB. The antenna elements in the proposed configuration have isolation better than −20 dB which assures that the work of this article is highly suitable for unitterupted wireless communications.

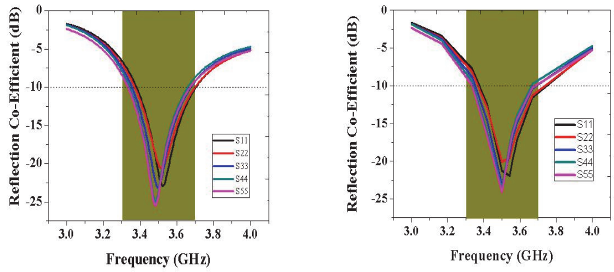

Figure 3 Scattering parameters co-efficients performance illustrations

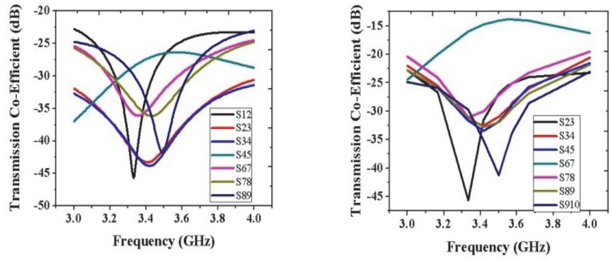

Figure 4 Simulated and measured transmission co-efficients

To improve isolation between adjacent antennas in a MIMO design, several techniques can be applied. Increasing the physical spacing between antenna elements, ideally at least half a wave length, reduces mutual coupling and enhances isolation. Additionally, placing antennas in orthogonal orientations, such as vertical-horizontal or cross-polarized configurations, can further minimize direct coupling. Implementing a notched or slotted ground plane around the antennas helps control the current distribution and reduce interference. Decoupling networks, including isolation resistors, can be integrated between antennas to decrease coupling. Utilizing polarization diversity, where adjacent antennas use orthogonal polarizations, also improves isolation. Finally, introducing physical shielding, like metallic or dielectric barriers, between elements can block unwanted signals and further enhance isolation. These combined methods ensure better MIMO performance and reduced interference in compact designs.

3.2 Performance Estimation

The effects of varying slot lengths ($L1$ and $L2$) are demonstrated through Fig. 5. Enlarging the slot lengths ($L1$ and $L2$) results in a leftward shift (lower frequency) of the operating frequency throughout the spectrum, and vice versa. This shift is primarily influenced by varying the slot length, which produces the significant performance.

In Fig. 5a, the length ($L2$) has been varied from 8.8 to 10.3 mm in 0.5 mm increments which causes it has been shifted towards the left. Similarly, Fig. 5b illustrates a similar response when slot length $L2$ is changed from 0.2 to 1.2 mm. Additionally, Fig. 5c demonstrates that variations in the feeding strip length (Lf) significantly impact the frequency resonance and impedance matching, causing shifts in the operating frequency.

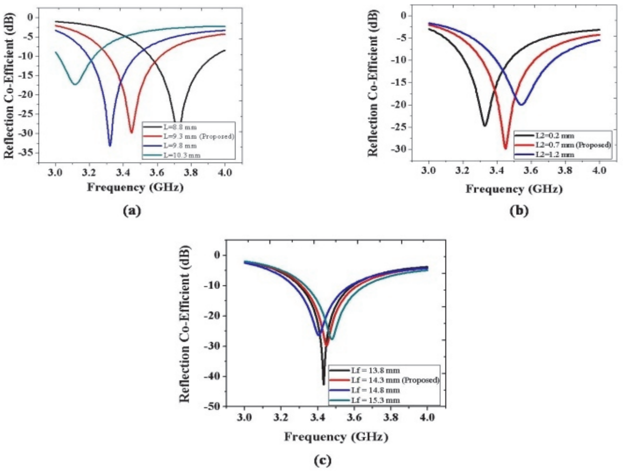

Figure 5 Simulated eeflection co-efficients when changing (a) *L*1, (b) *L*2, (c) *Lf*

3.3 Surface Current Distribution

The investigation of ground plane surface current was conducted to examine the factors contributing to the antenna components. At frequency 3.5 GHz, the activation of Ant1 is performed to obtain the corresponding surface current in the ground plane which remains stationary, indicating a significant level of isolation, as depicted in Fig. 6. Notably, the distribution of current with a sharp decrease in current strength beyond the excited antenna. This effectively limits electromagnetic interference with neighboring radiated elements. The maximum current density is observed near the trailing edge of the slot when Antenna 1 is stimulated at 3.5 GHz, as shown in Fig. 6. In the resonant mode, the current at the open end is zero, where the slotted antenna reaches its maximum at the opening and through the trailing edge that has low value. Fig. 6 illustrates the performance at the frequency of 3.5 GHz. This verifies that the open-ended slotted antenna operates in its fundamental mode of $\lambda/4$.

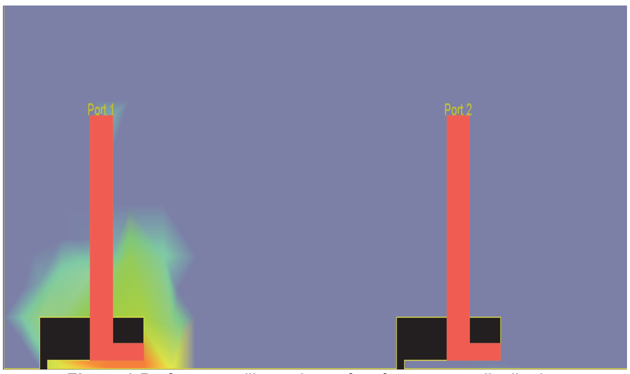

Figure 6 Performance illustrations of surface current distribution

Different notch configurations affect key parameters, including impedance matching, bandwidth, and radiation efficiency. By adjusting the current distribution on the ground plane, notches can broaden bandwidth and enhance resonance at specific frequencies. Certain notch shapes and placements can also improve isolation in MIMO configurations by reducing unwanted coupling between elements. This design flexibility makes it essential to assess how each notching pattern influences overall antenna performance.

3.4 Radiation Pattern, *ECC* and TARC Analysis

The designed MIMO antenna arrays in 5G smart phone are located nearby. Hence, there is a chance of forming interference between the antenna elements in designed 5G smart phone. The interference should be minimum for obtaining better performance. Interference is categorized as Cross-polarization (Etheta) and Co-polarization (Ephi). It is desirable for the cross-polarization between the designed antenna elements to be minimized, while the co-polarization between them should be maximized to the greatest extent.

The co-polarization and cross-polarization values are key indicators of the antenna's polarization performance. Co-polarization refers to the component of the signal that aligns with the desired polarization, typically resulting in higher signal strength and optimal performance. In contrast, cross-polarization represents the unwanted signal component that is perpendicular to the co-polarization, leading to lower signal strength and reduced performance. The co-polarization value is usually stronger, and for circularly polarized antennas, the axial ratio (AR) is used to quantify polarization quality, with an ideal AR of less than 3 dB indicating minimal cross-polarization and efficient co-polarization. These values depend on the antenna design and operating conditions, and achieving low cross-polarization while maintaining strong co-polarization is crucial for ensuring high efficiency and signal integrity.

All the antenna elements having omni-directional radiation pattern along phi and theta direction have been depicted in Fig. 7a and Fig. 7b.

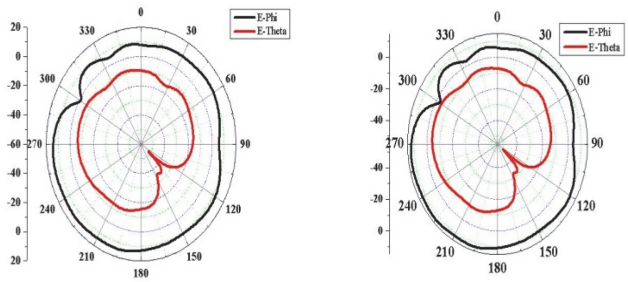

Figure 7(a) Simulated radiation pattern (b) Measured radiation pattern (Ant 1 excited)

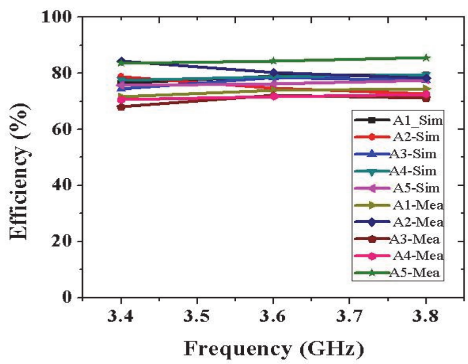

Figure 8 Simulated efficiency of Ant 1 - 5

The radiation efficiencies of proposed antenna for antenna 1 to 5 are shown in Fig. 8 and they range from 78 - 79 across the desired range of operation.

This section also investigates the related Envelope Correlation Coefficient (*ECC*), TARC and Channel

Capacity (CC) to validate the MIMO performance with respect to various parameters.

3.5 *ECC*

The technique used to calculate the *ECC* of the proposed antenna involves deriving *ECC* values from the simulated S-parameters. This method uses the S-parameter approach, which calculates *ECC* based on the complex scattering parameters (S-parameters) of the antenna ports. By analyzing the S-parameter data, *ECC* can be accurately determined without relying on complex 3D far-field radiation patterns, offering a simpler and effective way to assess the diversity performance and isolation of the MIMO antenna.

The user tested the 5G smartphone design with different postures to evaluate its radiation pattern performance. By changing the orientations of the smartwatch, scattering propagation is created. The scattering propagation of the designed 5G smartphone is analyzed using the *ECC* parameter, which should have a low value to ensure high efficiency. The below equation describes the computations of the *ECC* parameter.

$$ECC = \frac{\left|\iint R_1 \cdot R_2 \cdot \mathrm{d}\omega\right|^2}{\iint |R_1|^2 \, \mathrm{d}\omega \cdot \iint |R_2|^2 \, \mathrm{d}\omega}$$

The radiation patterns are referred to as R_1 and R_2, respectively. It has been noticed that *ECC* value would be less than 0.05. The maximum *ECC* throughout has been just 0.02, which is significantly much substandard to admissible benchmark of Envelope Correlation co-efficient less than 0. 5.

3.6 Channel Capacity

The recommended antenna array's ergodic channel capacity is determined through 100000 independently distributed random channels in this paper. The communication system lacks Channel State Information (CSI) in both the transmitting and receiving ends. They exhibit very low loss in the 10-port MIMO system. The suggested antenna array's ergodic channel capacity ranges between 49.8 and 51.2 b/s/Hz, depicted in Fig. 9.

3.7 TARC

The designed antenna array in 5G smart phone is measured by TARC. The value of the obtained TARC must be low (−10 dB below) for obtaining a better performance of the designed 5G smart phone. As illustrated in Fig. 9c, the Total Active Reflection co-efficient has been plotted for port 1 by changing the phase of the other ports without changing the amplitude of all other ports. While altering the excitation phases, the recommended MIMO antenna array pattern may span the appropriate frequency band with 2:1 VSWR. This demonstrates that the suggested architecture is ideal for 5G MIMO mobile phones.

Fig. 9a depicts the Gain performance illustrations and the antenna that has overall gain across the proposed antenna around 3.95 dBi to 4.25 dB is which is highly adequate for 5G mobile phone applications.

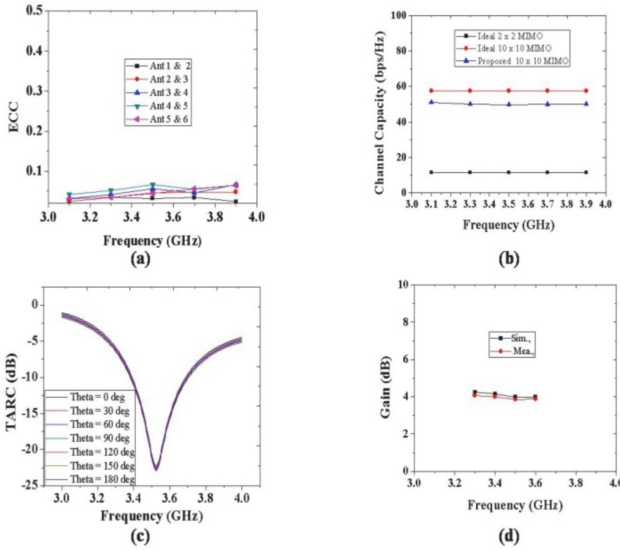

Figure 9 (a) *ECC*, (b) Channel capacity, (c) TARC, (d) Gain

3.8 Hand Phantom Analysis

The use of small antennas in mobile handsets can be adversely affected by the user's hand and head, leading to detuning, reduced radiation efficiency, and altered resonances. To mitigate these effects, antenna designs can be optimized for broadband performance, ensuring efficiency across a wide range of frequencies despite user interference. Implementing artificial ground planes or meta materials can enhance impedance matching and radiation efficiency, while adaptive impedance matching circuits allow dynamic compensation for changes caused by hand and head proximity. Additionally, using multiple antenna elements in a MIMO configuration helps maintain signal integrity by compensating for performance degradation in one element. Hand detection algorithms can also adjust antenna parameters in real-time to counteract the effects of hand and head interactions. Proper antenna placement and orientation, along with flexible or conformal designs, allow antennas to better adapt to user positioning, ensuring consistent performance and efficiency. These strategies collectively help improve the antenna's robustness and maintain optimal performance in real-world conditions.

This section examines the effects of the hand phantom. Fig. 10a and Fig. 10b depict two standard possible applications: Single-Hand Configuration (SHC) and Dual-Hand Configuration (DHC). Fig. 11 and Fig. 12 show the respective simulated performance measures for the two mechanisms, SHC and DHC.

Notably, it is important to highlight that the multiport MIMO operation at frequencies below 6 GHz is intended solely for data transmission and not for voice transmission. Therefore, the involvement of user or human with hand is not taken into account. Antennas 2, 6, and 7 come into direct handling by hand in mobile application purposes. This specific arrangement has a significant impact on the return losses of Antennas 2, 6, and 7, as depicted in Fig. 11a. Antenna 6, in particular, exhibits poor impedance matching in this configuration. Due to their relative distance from the fingers, Antennas 1, 4, 5, and 8 exhibit slight variations in resonance frequencies. However, Fig. 11b illustrates that a high level of isolation (> 17 dB) can be maintained across the operational spectrum.

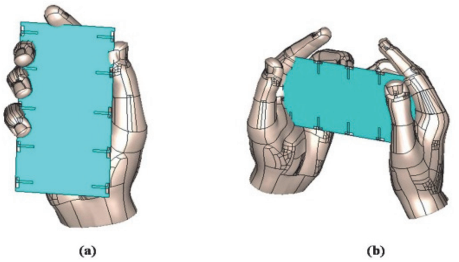

Figure 10 (a) SHC, (b) THC

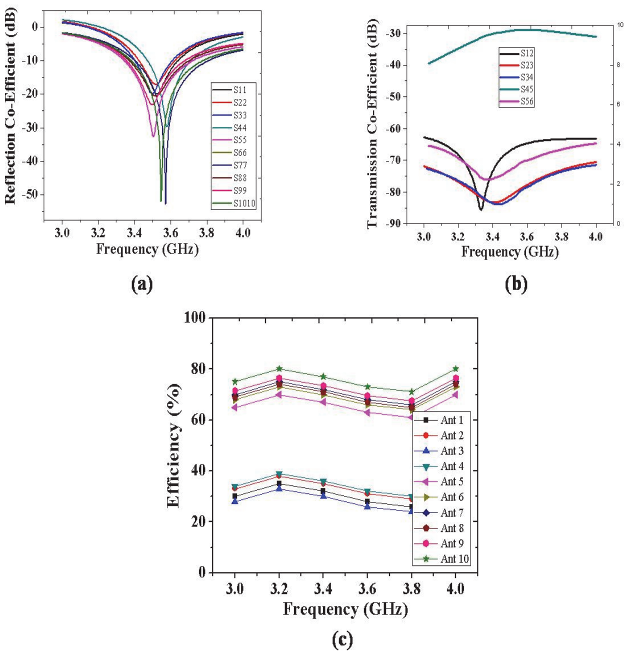

Figure 11 Performance of the antenna under the influencre of SHO (a), (b) S-Parameters, (c) Efficiency

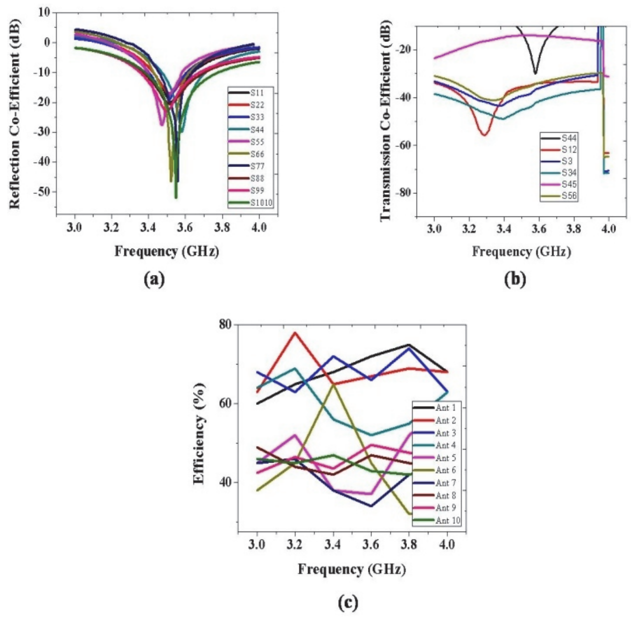

Figure 12 Performance of the antenna under the influencre of THO (a), (b) S-Parameters, (c) Efficiency

The process involves placing a human body model or a phantom in front of an antenna and using a receiver or field probe to detect the radiated power from the antenna. The measurements are taken at various angles relative to the antenna's radiating element to capture the radiation pattern, focusing on the rear or backward direction (typically 180° opposite the antenna's main beam). The specific absorption rate (*SAR*) is another related measure, which quantifies the power absorbed by the human body from electromagnetic fields, providing insights into the intensity of radiation that interacts with the body. In these tests, electromagnetic field probes, such as E-field or H-field probes, are used to measure the electric or magnetic field strength, and the results are then used to calculate the backward radiation intensity based on the geometry and frequency of operation.

The specific absorption rate (*SAR*) is a crucial factor which measures the radiation levels into the human body. The *SAR* for the proposed antenna has been simulated by inculding headphantom in the simulation and verified the maximum values at 1g and 10g of human tissues as shown in Fig. 13. The values of *SAR* for different antenna ports listed in Tab. 1 prove that the proposed antenna has satisfies the norms recommended by FCC.

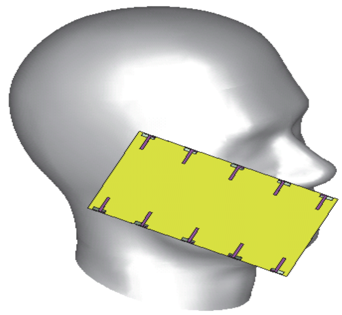

Figure 13 Proposed antenna with head Phantom for *SAR* analysis

Table 1 *SAR* of antenna ports

Antenna Ports	*SAR* / W/Kg	
	1 g	10 g
1	1.235	0.9875
2	1.1564	0.9654
3	1.2365	0.9875
4	1.32	0.994
5	1.1456	1.01

To maintain the efficiency of antenna elements in the presence of hand effects, several strategies can be employed. Positioning the antenna away from the hand or orienting it to minimize direct interaction with the body can help reduce detuning. Additionally, tuning the antenna to have a broader frequency range or implementing adaptive impedance matching allows the antenna to compensate for the changes caused by hand proximity. Incorporating neutralizing structures like ground planes or decoupling capacitors can help mitigate the effects by providing alternative pathways for radiated power. Using multiband or multiple antenna elements with different orientations ensures that if one element is affected by hand interference, others can maintain performance. Finally, employing flexible or conformal antenna designs, especially in wearable devices, allows the antenna to adapt to varying hand positions, ensuring consistent efficiency. These techniques collectively help maintain optimal antenna performance despite the presence of hand effects.

It is essential to clarify that the placement of antenna elements significantly impacts the overall performance of the MIMO system, particularly in terms of isolation, gain, and efficiency. Proper spacing between elements minimizes mutual coupling, which reduces interference and enhances signal clarity. Ideally, elements are placed at intervals of at least half a wavelength of the operating frequency to ensure low mutual coupling, which improves the envelope correlation coefficient (*ECC*) and diversity gain. Placement also affects the beam forming capabilities and pattern diversity of the antenna, which are critical for achieving high data throughput and reliability in mobile environments. For compact designs, such as those used in mobile phones, careful element positioning and orientation are required to maintain performance without exceeding space limitations. Thus, strategic placement is crucial to optimizing MIMO performance, ensuring minimal signal degradation, and achieving high data transmission rates.

Tab. 2 compares the performance of the work proposed in this atricl with few relevant works already published. It revelas the 10- port antenna designed in this work has better performance in all aspects related to radiation charecteristics with other antennas.

Table 2 Antenna geometric parameters comaparison

Ref. No	Operating frequency / GHz	Size of the antenna / mm^2	Frequency span / GHz	Isolation / dB	Correlation Coefficient	Radiation Efficiency / %
[3]	3.5	7 × 12	3.4 - 3.6 (−6)	> 17	< 0.07	49-61
[4]	3.5	9.5 × 12	3.4 - 3.6 (−10)	> 10	< 0.2	62-78
[5]	3.5	4.9 × 12.5	3.3 - 3.6 (−6)	> 15	< 0.15	60
[8]	3.5	28.4 × 1	3.4 - 3.6 (−6)	> 15	< 0.2	40-55
[9]	3.45	12 × 12	3.3 - 3.6 (−6)	> 10	< 0.11	64.2-73.2
[10]	3.5	7 × 10	3.3 - 3.6 (−6)	> 10	< 0.11	48.6-73.2
[11]	3.5	40.8 × 3	3.4 - 3.6 (−6)	> 11.6	–	47-51
[16]	3.6	45.2 × 5	3.3 - 3.9	18	< 0.005	60-80
[17]	3.1	39.8 × 6	2.5 - 3.6	> 10	< 0.02	45 - 65
[18-20]	3.4 - 3.6	13.25 × 5	3.4 - 3.6	> 20	< 0.4	33 – 47
This Work	3.5	9.3 × 3	3.32 - 3.62 (−10)	> 20	< 0.03	70-74

4 CONCLUSIONS

This study presents a 10-port mobile antenna which has been designed for higher mobile application devices. By strategically arranging the antenna components, effective isolation between them can be achieved. This design performs well within the 3.5 GHz range (3.4 - 3.6 GHz), exhibiting isolations below 17.5 dB, radiation efficiency exceeding 62%, and minimal error correction coding (*ECC*) of 0.05. Channel capacity calculations have been conducted for the proposed 10-port antenna array at 20 dB SNR. Notably, the antenna has demonstrated strong robustness when affected by the user's hand. Considering these qualities, the researched antenna holds considerable potential for future 5G mobile phone applications.The future work could focus on using advanced materials to further miniaturize the antenna while maintaining performance and optimizing element placement for better isolation in different device layouts. Additionally, adaptive algorithms to adjust antenna parameters based on usage conditions could further enhance signal quality. These improvements would support the evolving demands of mobile communication systems.

5 REFERENCES

[1] Hong, W. (2017). Solving the 5G mobile antenna puzzle: Assessing future directions for the 5G mobile antenna paradigm shift. *IEEE Microwave Magazine, 18*(7), 86-102. https://doi.org/10.1109/MMM.2017.2740538

[2] Li, Y., Sim, C. Y .D., Luo, Y., & Yang, G. (2018). 12-port 5G massive MIMO antenna array in sub-6GHz mobile handset for LTE bands 42/43/46 applications. *IEEE Access, 6*, 344-354. https://doi.org/10.1109/ACCESS.2017.2763161

[3] Sun, L., Feng, H., Li, Y., & Zhang, Z. (2018). Compact 5G MIMO mobile phone antennas with tightly arranged orthogonal-mode pairs. *IEEE Transactions on Antennas and Propagation, 66*(11), 6364-6369. https://doi.org/10.1109/TAP.2018.2864674

[4] Sudha, R. & Bhavani, S. (2024). Efficient MIMO Antenna Design Using Metamaterials for Compact and High-Performance Communication Applications. *Tehnički vjesnik, 31*(5), 1719-1725. https://doi.org/10.17559/TV-20231227001236

[5] Parchin, N. O., Al-Yasir, Y. I. A., Ali, A. H., Issa, E., James, M. N., & Jonathan, R. (2019). Eight-element dual-polarized MIMO slot antenna system for 5G smartphone applications. *IEEE Access, 9*, 15612-15622. https://doi.org/10.1109/ACCESS.2019.2893112

[6] Ban, Y. L., Li, C., Sim, C. Y. D., Gang, W., & Kin-Lu, W. (2016). 4G/5G multiple antennas for future multi-mode smartphone applications. *IEEE Access, 4*, 2981-2988. https://doi.org/10.1109/ACCESS.2016.2582786

[7] Zhang, S., Ying, Z., Xiong, J., & He, S. (2009). Ultrawideband MIMO/diversity antennas with a tree-like structure to enhance wideband isolation. *IEEE Antennas and Wireless Propagation Letters, 8*, 1279-1282. https://doi.org/10.1109/LAWP.2009.2037027

[8] Zhang, S., Lau, B. K., Tan, Y., Ying, Z., & He, S. (2012). Mutual coupling reduction of two PIFAs with a T-shape slot impedance transformer for MIMO mobile terminals. *IEEE Transactions on Antennas and Propagation, 60*(3), 1521-1531. https://doi.org/10.1109/TAP.2011.2180329

[9] Ban, Y. L., Li, C., Sim, C. Y. D., Wu, G., & Wong, K. L. (2016). 4G/5G multiple antennas for future multi-mode smartphone applications. *IEEE Access, 4*, 2981-2988. https://doi.org/10.1109/ACCESS.2016.2582786

[10] Li, Z., Du, Z., Takahashi, M., Saito, K., & Ito, K. (2012). Reducing mutual coupling of MIMO antennas with parasitic elements for mobile terminals. *IEEE Transactions on Antennas and Propagation, 60*(2), 473-481. https://doi.org/10.1109/TAP.2011.2173127

[11] Lee, J. Y., Kim, S. H., & Jang, J. H. (2015). Reduction of mutual coupling in planar multiple antennas by using 1-D EBG and SRR structures. *IEEE Transactions on Antennas and Propagation, 63*(9), 4194-4198. https://doi.org/10.1109/TAP.2015.2434397

[12] Jiang, W., Liu, B., Cui, Y. Q., & Wei, H. (2019). High-isolation eight-element MIMO array for 5G smartphone applications. *IEEE Access, 7*, 34104-34112.

https://doi.org/10.1109/ACCESS.2019.2904647

[13] Liu, Y., Ren, A. D., Liu, H., Hanyang, W., Chow-Yen-Desmond, S. (2019). Eight-port MIMO array using characteristic mode theory for 5G smartphone applications. *IEEE Access, 7*, 45679-45692. https://doi.org/10.1109/ACCESS.2019.2909070

[14] Sun, L. B., Feng, H. G., & Li, Y. (2018). Tightly arranged orthogonal mode antenna for 5G MIMO mobile terminal. *Microwave and Optical Technology Letters, 60*(7), 1751-1756. https://doi.org/10.1002/mop.31283

[15] Wong, K. L., Tsai, C. Y., & Lu, J. Y. (2017). Two asymmetrically mirrored gap-coupled loop antennas as a compact building block for eight-antenna MIMO array in the future smartphone. *IEEE Transactions on Antennas and Propagation, 65*(4), 1765-1778. https://doi.org/10.1109/TAP.2017.2670534

[16] Deng, C. J., Liu, D., & Lv, X. (2019). Tightly-arranged four-element MIMO antennas for 5G mobile terminals. *IEEE Transactions on Antennas and Propagation, 7*(10), 6353-6361. https://doi.org/10.1109/TAP.2019.2922757

[17] Parchin, N. O., Al-Yasir, Y. I., Basherlou, H. J., Abd-Alhameed, R. A., & Noras, J. M. (2020). Orthogonally dual-polarized MIMO antenna array with pattern diversity for use in 5G smartphones. *IET Microwaves, Antennas & Propagation, 14*(6), 457-467. https://doi.org/10.1049/iet-map.2019.0328

[18] Abdullah, M., Kiani, S. H., & Iqbal, A. (2019). Eight-element multiple-input multiple-output (MIMO) antenna for 5G mobile applications. *IEEE Access, 7*, 134488-134495. https://doi.org/10.1109/ACCESS.2019.2941566

[19] Li, R., Mo, Z., Sun, H., Sun, X., & Du, G. (2020). A low-profile and high-isolated MIMO antenna for 5G mobile terminal. *Micromachines, 11*(4), 360-372. https://doi.org/10.3390/mi11040360

[20] Krishnamurthi, M. & Kalimuthu, V. K. (2024). Enhancing Spectrum Sharing Efficiency in Large-Scale MIMO Systems over Integration of Cognitive Radio and Reinforcement Learning. *Technical Gazette, 31*(5), 1536-1543. https://doi.org/10.17559/TV-20230908000926

Contact information:

R. S. MATHU BALA, Assistant Professor
(Corresponding author)
Department of ECE,
Vivekanandha College of Engineering for Women (Autonomous),
Tiruchengode, Tamil Nadu, India
E-mail: mathubala1991@gmail.com

K. THENMALAR, PhD Professor
Department of EEE,
Vivekanandha College of Engineering for Women (Autonomous),
Tiruchengode, Tamil Nadu, India
E-mail: thenmalark@gmail.com